J. Fluid Mech. (1974), *vol.* 64 *part* 3, *pp.* 507–527
Printed in Great Britain

The evolution of under-ice melt ponds, or double diffusion at the freezing point

By SEELYE MARTIN
Department of Oceanography, University of Washington, Seattle
AND PETER KAUFFMAN
Department of Atmospheric Sciences, University of Washington, Seattle

(Received 14 August 1973)

In an experimental and theoretical study, we model a phenomenon observed in the summer Arctic, where a fresh-water layer at a temperature of 0 °C floats both over a sea-water layer at its freezing point and under an ice layer. Our results show that the ice growth in this system takes place in three phases. First, because the fresh-water density decreases upon supercooling, the rapid diffusion of heat relative to salt from the fresh to the salt water causes a density inversion and thereby generates a high Rayleigh number convection in the fresh water. In this convection, supercooled water rises to the ice layer, where it nucleates into thin vertical interlocking ice crystals. When these sheets grow down to the interface, supercooling ceases. Second, the presence of the vertical ice sheets both constrains the temperature T and salinity s to lie on the freezing curve and allows them to diffuse in the vertical. In the interfacial region, the combination of these processes generates a lateral crystal growth, which continues until a horizontal ice sheet forms. Third, because of the T and s gradients in the sea water below this ice sheet, the horizontal sheet both migrates upwards and increases in thickness. From one-dimensional theoretical models of the first two phases, we find that the heat-transfer rates are 5–10 times those calculated for classic thermal diffusion.

1. Introduction

When a fresh-water layer floats over a sea-water layer and under an ice sheet with the temperatures of both layers very near their respective freezing points, the heat transfer between the two layers generates ice. In nature, this phenomenon occurs in at least two places. The first is under the polar pack ice during the arctic or austral summer; the second, at the bottom of the Ward Hunt Ice Shelf during the arctic summer.

For the pack-ice case, the fresh water is generated by the summer solar radiation melting the fresh ice on the surface of the pack. Untersteiner (1967) estimates that during the arctic summer 30 cm of ice ablation occurs on average over an area of $10^7\,\mathrm{km}^2$. A large part of this fresh melt water flows off the pack and into the ocean, where part of it is swept under the ice and trapped in inverted

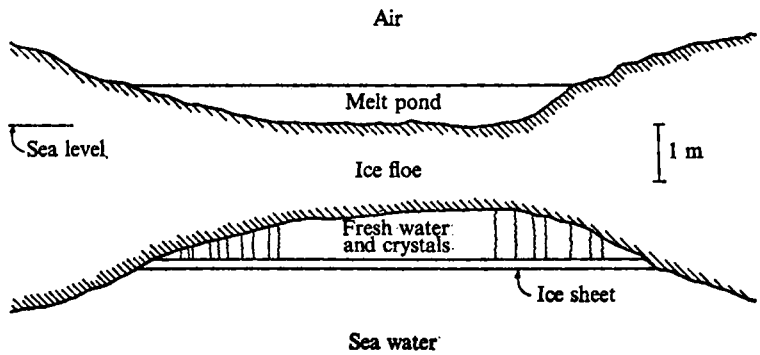

FIGURE 1. A schematic diagram of an under-ice melt pond, drawn from Hanson's (1965) description.

hollows in the bottom, forming what Hanson (1965) calls 'under-ice melt ponds'. From his observations in the Beaufort Sea, Nansen (1897) first pointed out that the heat transfer from the trapped fresh water, with a temperature of 0 °C, to the arctic sea water, with a temperature of − 1·6 °C, is the only source of ice accretion during the polar summer.

A similar process occurs under the Ward Hunt Ice Shelf (latitude 74° W, longitude 83° N) on northern Ellesmere Island. As Lyons, Savin & Tamburi (1971) discuss, this ice shelf serves as a dam to a depth of about 40 m across the mouth of Disraeli Fjord. In the summer, fresh-water glacial run-off at a temperature very near 0 °C accumulates behind the ice shelf until the fresh water flows out beneath the shelf over the − 1·6 °C arctic sea water. Lyons *et al.* estimate that 20 cm yr^{-1} of ice form under the shelf from the heat transfer between the salt and fresh water and that this freezing maintains the mass balance of approximately 10^2 km^2 of the ice shelf.

Because of their accessibility, there are numerous observations on how freezing occurs in the under-ice melt ponds. Authors such as Zubov (1945, §§ 42–43), who summarizes earlier observations, Untersteiner & Badgley (1958) and Hanson (1965) state from surface observations that freezing creates a solid sheet of ice of thickness 2–10 cm at the interface between the fresh and salt water. They also note that loosely packed ice crystals fill the fresh water in the space between the bottom of the pack ice and the ice sheet. Figure 1 is a schematic diagram of an under-ice melt pond based on their observations.

Divers have also directly observed these under-ice ponds. Campbell (1973, private communication) reports from observations made while diving in the Beaufort Sea during the summer of 1958 that these under-ice ponds were numerous, with typical horizontal dimensions of 5–10 m. On one occasion, Campbell poked his head up through the ice sheet covering the bottom of the pond and described the pond as follows. The ice sheet had a uniform thickness of about 5 cm; the bottom of this sheet was flat, with relief of the order of 1–2 mm. Inside the melt pond, which had a depth of about 60 cm, thin vertical crystals ran from the bottom of the pack ice to the top of the ice sheet. These crystals measured 1–2 cm in width and were less than 1 mm thick. In a horizontal cross-

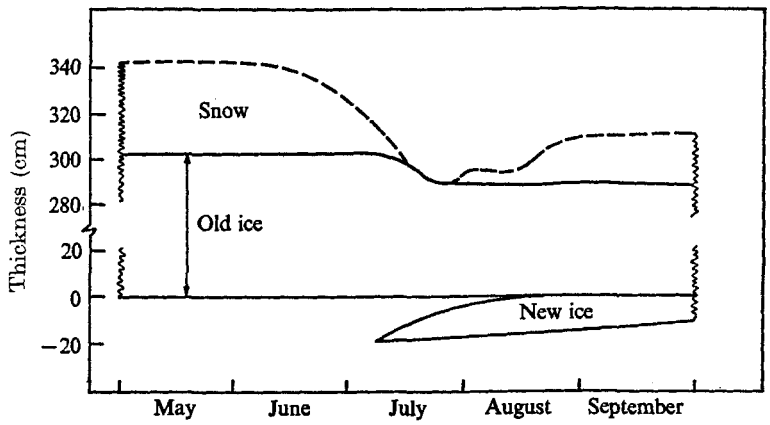

FIGURE 2. A diagram of both the changes in total ice thickness and the growth of ice in an under-ice melt pond during the summer of 1957 at Drifting Station A in the Beaufort Sea (adapted from figure 4 of Untersteiner & Badgley 1958).

section, the crystals were randomly oriented and intersected one another with a typical spacing of about 1 cm. They occupied 5–10 % of the volume of the fresh water.

There are also two observations of the development of these melt ponds in time. Both Untersteiner & Badgley (1958) and Hanson (1965) report that the horizontal ice sheets forming the bottom of the melt ponds migrate upwards. Figure 2, which is taken from Untersteiner & Badgley, shows that throughout the summer the sheet both migrated upwards and increased in thickness. Hanson also observed upward migration, at a rate of order 1 cm day^{-1}, although in his observations, the ice thickness remained nearly constant.

All observers attribute the ice formation to the temperature difference between the fresh and salt water; in the present paper, we wish to describe the convective and diffusive processes by which this heat transfer takes place. In the next section, we describe an experiment which models the observed features of the under-ice ponds; then in the following sections we present three one-dimensional heat-transfer models which describe the various phases in the evolution of these ponds. Comparison of these one-dimensional models with the experiment suggests that the rate of heat transfer in the phases leading to the formation of the horizontal ice sheet is 5–10 times that predicted from classical heat-transfer theory.

2. The laboratory experiment

In modelling the ice growth, the important parameters are the temperature and salinity difference between the fresh and salt water and the depth and width of the fresh-water layer. From field observations, the surface sea-water salinity ranges from 26–28 ‰ in the Arctic to 34 ‰ in the Antarctic; the depth of the fresh water in the under-ice ponds is of order 1 m, and the width ranges from 10 m for the ponds to perhaps 1 km for the Ward Hunt Ice Shelf. With the

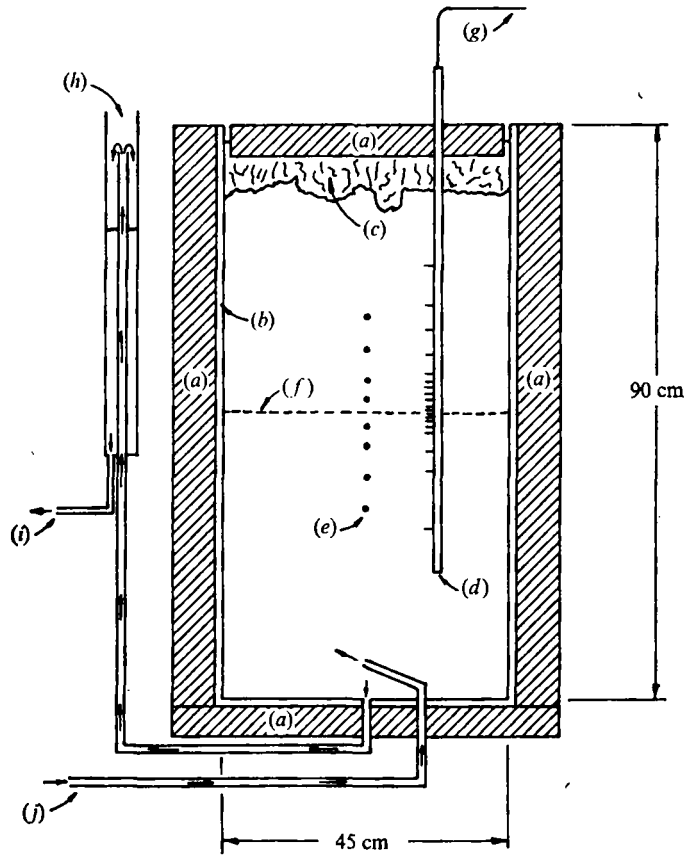

FIGURE 3. A schematic diagram of the apparatus. (*a*) Polyurethane insulation; (*b*) Plexiglas tank; (*c*) granular ice crystals; (*d*) thermocouple array; (*e*) holes for salinity sampling; (*f*) position of the initial interface; (*g*) cable to the digitizer; (*h*) overflow control; (*i*) to the salt-water reservoir; (*j*) from the salt-water reservoir.

exception of the width scale, we can easily model these conditions in the laboratory.

Figure 3 is a schematic diagram of our apparatus. We built both the tank and the thermocouple mount from clear acrylic plastic (Plexiglas). Compared with the thermal properties of water, the thermal conductivity of Plexiglas (4×10^{-4} cal (gm cm s)$^{-1}$) is an order of magnitude smaller; the thermal diffusivity (1×10^{-3} cm^2 s^{-1}), slightly smaller (from Perry, Chilton & Kirkpatrick 1963, table 23–7*a*). Therefore, the vertical heat transfer in the tank took place preferentially in the water rather than in the Plexiglas.

The tank, which had a cross-sectional area of 45 × 45 cm and a depth of 90 cm, was insulated with 10 cm thick sheets of polyurethane foam and placed in a cold room whose temperature stayed between $-0{\cdot}5$ and $-1{\cdot}5$ °C. At the beginning of the experiment, we filled the tank to a depth of 45 cm with 90 l of 34‰ NaCl solution. This salt solution was then cooled to its freezing point of $-1{\cdot}9$ °C. Over the salt water, we carefully poured a 35 cm deep layer of fresh water with

a temperature of 0·75 °C. To minimize the turbulent mixing during the addition of the fresh water, we floated a porous raft on top of the salt water, then slowly poured the fresh water onto the raft. After completion of this process, we removed the raft, then added about 5 kg of granular fresh ice to the fresh water to bring the total depth of the ice–fresh-water mixture to 40 cm. On top of this mixture, we anchored a polyurethane foam raft which supported our thermocouple array.

To maintain the salt water at its freezing point, we constantly circulated the salt water between the experimental tank and a 50 l reservoir. The reservoir was both vigorously stirred and buffered with a block of ice maintained by a cold bath to keep the salt-water temperature at $-1{\cdot}9$ °C. Before entering the tank, the salt water flowed through an air-bubble trap. Then, as figure 3 shows, the salt water entered the experimental tank through a slanted inlet pipe, circulated around inside the tank and left through a drainage hole in the bottom. The turnover time of the salt water in the tank was about 2 h. The water then passed through an overflow and returned to the cooling tank. From dye observations, we found that the fluid below the density interface moved in a large laminar eddy. The density change across the interface inhibited the transfer of this motion to the fresh water.

To measure the temperature profiles inside the experimental tank, we used a thermocouple array. This array consisted of 19 copper–constantan thermocouples which were mounted vertically inside the tank on a Plexiglas support at a distance of about 15 cm from the front wall at the depths shown in figure 3. To avoid heat losses through the thermocouple leads, we encased them inside the Plexiglas support, which in cross-section measured $4 \times 0{\cdot}8$ cm. The individual thermocouples, which were enclosed inside glass tubes with an outer diameter of 10^{-1} cm, extended perpendicularly from the broad side of the support. The thermocouple junctions were located 1 cm from the support in the ends of the glass tubes, and the thermocouples at different heights were offset in the horizontal so that they did not lie directly above one another. An additional thermocouple inside the cold room measured the room temperature. A Dewar flask, filled with a mixture of crushed ice and distilled fresh water, held the 0 °C reference junction for the array. A digitizer sequentially scanned the output from these thermocouples at 20 min intervals throughout the experiment, so that the temperatures were digitized and recorded on magnetic tape for subsequent listing. The accuracy of these temperature measurements was $\pm 1\,\mu$V or $\pm 2{\cdot}5 \times 10^{-2}$ °C.

To measure the salinity profiles, we withdrew water samples from the tank. Figure 3 shows the positions of the sampling holes, which were located on the back wall of the tank. We plugged these holes, which had diameters of 0·64 cm and lengths of 1·3 cm, with an elastic sealant called Dow Corning 732 RTV Silastic. To take samples, we inserted a hypodermic needle with an outer diameter of 0·125 cm and length of 7·6 cm through the plugs and then removed samples with a syringe. Because the needle diameter was much less than the hole diameter, we could tilt the needle up or down and thus vary our sampling level. A ruler mounted next to the holes on the outside of the tank allowed us to

position the needle to within a millimetre. When we withdrew the needle, the plug immediately resealed itself without leaking. We then measured the sample salinity using an American Optical refractometer which was accurate to $\pm 0{\cdot}5\,‰$.

We recorded the ice growth photographically. In the photographs, the axis of our camera lens is level with the initial interface height. To increase contrast between the ice crystals and the water, we lit the interior of the tank with a diffuse polarized light source. We then mounted a polarizing filter on our camera lens, and rotated the filter to increase the contrast between the ice crystals and the water. Figure 4 (plate 1), which is an enlargement of the crystals which initially formed in the tank, shows the shading induced by the polarized light.

The photographs also qualitatively record the salinity profile. Following Mowbray (1967), on day 5 of the experiment, we mounted two straight pieces of tape at angles of about 45° to the vertical on the outside of the back wall of the tank. The index-of-refraction jump caused by the salinity gradient distorted these straight lines into irregular lines on the photographs.

The experiment began when we finished filling and assembling the tank at 1500 h on 6 March 1973, hereafter called day 1, and ended 36 days later. Figure 5 (plates 2 and 3) is a sequence of photographs from the experiment; figure 5 (*a*) shows the initial conditions. The experiment took place in three phases. Before giving a detailed discussion of each phase in the following sections, we shall briefly summarize them.

First, 14 h after the experiment began, the fresh water reached its freezing point. On days 2 and 3, as figures 5 (*b*) and (*c*) show, we observed both the growth of thin vertical crystal sheets from the bottom of the granular ice, and from our temperature and salinity data, supercooling at the interface. Our observations suggest that the fresh-water layer was convectively unstable, with the supercooled water rising from the interface to the surface, where nucleation occurred.

Second, at 1500 h on day 3, both the Plexiglas walls and the thermocouple mount served as nucleation sites for the supercooled water generated at the interface. As figure 5 (*d*) shows, thin vertical plates of ice formed on these sites near the interface. These ice plates subsequently began to grow laterally. This lateral growth, combined with some filling in of the interior of the tank, created a horizontal ice sheet on day 14. Figure 5 (*f*) shows the appearance of the ice shortly after the ice sheet formation.

Third, this horizontal ice sheet migrated upwards, with the bottom of the ice sheet becoming smooth and glassy about day 21. After this time, as figures 5 (*g*) and (*h*) show, the ice sheet both slowly increased in thickness and migrated upwards at a rate of $0{\cdot}2\ \mathrm{cm\ day^{-1}}$. The vertical lines in the ice sheet in these figures are air bubbles caused by the rejection of dissolved air from the water upon freezing.

Figure 6 summarizes the formation, growth and upward migration of the ice which formed at the interface. The lower points mark the bottom of the ice crystals and subsequent ice sheet; the upper points, the top. The gaps in the upper points occur where we could not identify a uniform height as the top of the vertical crystals. The vertical lines above the points divide the ice growth into four parts. The time period marked (*a*) denotes the initial convection, while

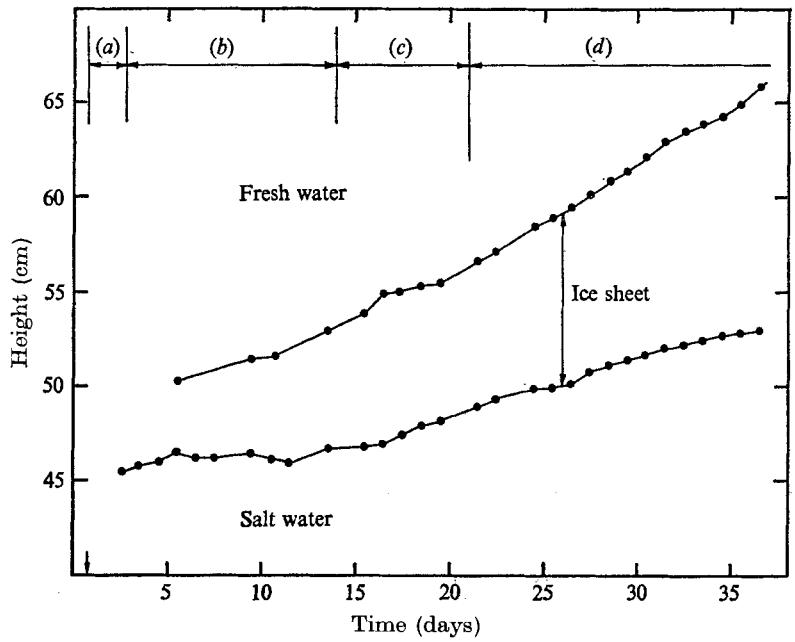

FIGURE 6. The observed position of the upper and lower boundary of the ice crystals and subsequent ice sheet which formed near the interface. The vertical scale measures height above the bottom of the tank; the horizontal scale gives the time in days measured from the calendar day (6 March 1973) on which the experiment began. The lower set of solid circles shows the observed position of the ice bottom; the upper set, the ice top. The arrow near the time origin marks the beginning of the experiment. The time periods (*a*), (*b*), (*c*) and (*d*) are explained in the text.

(*b*) denotes the formation and lateral growth of the vertical plates. The time periods (*c*) and (*d*) denote the upward migration of the ice sheet; in (*c*) the ice sheet bottom is rough, in (*d*) the bottom is flat. Once the ice sheet formed, we could measure the position of its bottom to within 5×10^{-2} cm, whereas we could only measure the top position to within 0·5 cm. The figure clearly shows the upward migration and increase in thickness of the ice sheet with time.

For theoretical purposes, the ice formation and growth took place in three phases: (i) the initial convection with vertical crystals growing down from the surface; (ii) the formation and subsequent lateral growth of vertical crystals at the interface; and (iii) the formation and upward migration of a horizontal ice sheet. In the following sections, we both present and compare with experiment one-dimensional models for each of these phases.

3. The initial convection

We assume that the experiment begins with a fresh-water layer at a temperature $T = 0\,^{\circ}\mathrm{C}$ floating over a salt-water layer of salinity $s = 34‰$ at a temperature of $-1{\cdot}9\,^{\circ}\mathrm{C}$. Carslaw & Jaeger (1959, hereafter abbreviated to CJ) show that the relative diffusion rates of these initial steplike profiles depend on the ratio

$$\alpha_1 = \kappa/D. \tag{1}$$

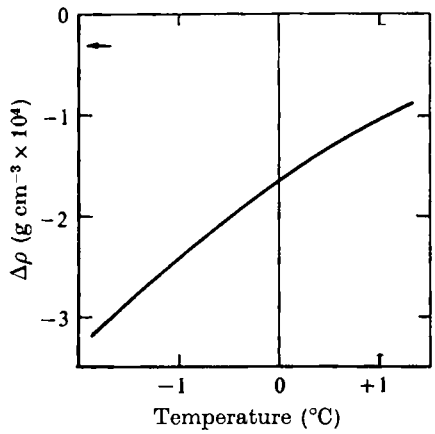

FIGURE 7. The temperature dependence of the density difference $\Delta\rho = \rho(T) - 1{\cdot}00000$ for fresh water in the approximate range $-1 \leqslant T \leqslant +1$ °C. The arrow marks the maximum density of fresh water (from Hodgman 1955, p. 1972).

From Kaufman (1960, chap. 25), both the salt and fresh water have a thermal diffusivity $\kappa = 1{\cdot}4 \times 10^{-3}\,\mathrm{cm^2\,s^{-1}}$ and a salt diffusivity $D = 7{\cdot}5 \times 10^{-6}\,\mathrm{cm^2\,s^{-1}}$, so that $\alpha_1 = 1{\cdot}9 \times 10^2$. For initial steplike profiles, CJ (chap. 2) shows that the ratio of the thickness z_T of the temperature transition layer to the thickness z_s of the salinity transition layer is

$$z_T/z_s = \alpha_1^{\frac{1}{2}} = 13{\cdot}6,$$

so that temperature diffuses an order of magnitude faster than salt.

Because the density of both fresh water and NaCl solutions with salinities less than 23‰ decreases with supercooling, both theory and our observations suggest that the upper half of this system is convectively unstable. For fresh water, figure 7 shows the temperature dependence of density around the freezing point. In the range $-1 \leqslant T \leqslant 0\,^\circ\mathrm{C}$,

$$\partial\rho/\partial T = \beta = 8 \times 10^{-5}\,\mathrm{g\,cm^{-3}\,^\circ C^{-1}},$$

where ρ is the density.

For these conditions, figure 8 compares the initial T, s and ρ profiles with their subsequent development. At the upper edge of the salinity transition layer, a zone of water forms which is both supercooled and the lightest water in the experiment. Because the density decrease caused by the temperature change from 0° to −1° equals the density increase caused by a salinity increase of 0·1‰ (Kaufman 1960, table 44), in our experiment supercooling produces a density inversion only for very small salinities.

Howard (1966), summarized in Turner (1973, § 7.3), describes the high Rayleigh number convection between widely separated parallel horizontal flat plates held at a constant potentially unstable temperature difference. Howard states that if the Prandtl number

$$P_r = \nu/\kappa > 1,$$

where for our experiment $\nu = 1{\cdot}8 \times 10^{-2}\,\mathrm{cm^2\,s^{-1}}$, so that $P_r = 14$, then convection occurs if

$$R_{a\delta} = \beta g \Delta T \delta^3/\kappa\nu \geqslant 10^3, \tag{2}$$

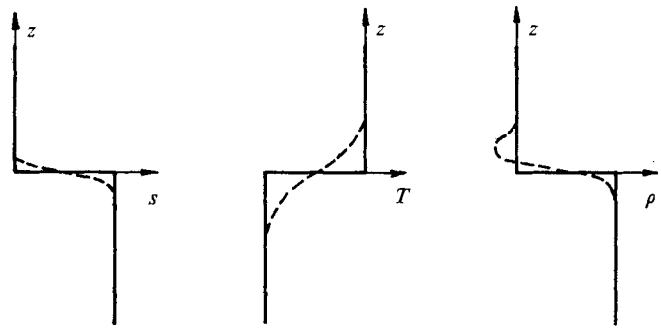

FIGURE 8. The distribution of (*a*) salinity, (*b*) temperature and (*c*) the resultant density caused by the diffusion of a fresh-water layer over a salt-water layer, with both layers at their respective freezing points. ——, initial profile; – – –, later profile. The size of the density inversion is exaggerated.

where ΔT is the temperature change across the boundary layer, g is the acceleration due to gravity and δ is the mean thickness of the unstable boundary layer.

Our problem differs from Howard's in two ways. First, our buoyancy source is not a constant-temperature plate, rather the thickness z_s of the salinity transition layer in part determines the buoyancy flux. Second, the buoyant water is supercooled, so that upon reaching a nucleation site, it crystallizes and thus causes downward ice growth. In spite of these differences, the similarity between the two problems suggests that (2) should also apply to our experiment.

To evaluate the magnitude of $R_{a\delta}$ in our case, we examine the salinity and temperature profiles displayed in figures 9(*a*)–(*c*). Figure 9(*a*) shows the initial conditions; figures 9(*b*) and (*c*) show the profiles which accompany the downward crystal growth. To show supercooling on these figures, we plot salinity as the temperature at which a solution of that salinity freezes, following Kaufman (1960, table 50). At those depths where the temperature is to the left of the salinity, the water is supercooled. From figures 9(*b*) and (*c*), the maximum observed supercooling in the fresh water is $2{\cdot}5 \times 10^{-1}$ °C and $\delta \simeq 1$–3 cm. Substitution of these values into (2) gives

$$R_{a\delta} = 10^3\text{–}10^4,$$

so that, by Howard's criterion, the interface is convectively unstable.

Figures 5(*b*) and (*c*) are photographs of the downward growth of the thin vertical crystal sheets taken on the same days as the s and T profiles shown in figures 9(*b*) and (*c*), and figure 4 is an enlargement of this crystal layer. As in Campbell's observations described in the introduction, the crystals were very thin sheets of ice, with a width of 1–4 cm. In most cases, the individual crystals grew in vertical sheets, with the plane of the sheets parallel to gravity, so that, in crystallographic terminology, the c-axis of the crystals was perpendicular to gravity. As the photographs suggest however, the planes of some of these crystals tipped as much as 45° away from the vertical. In a horizontal plane, the crystals were randomly oriented with a spacing of order 1 cm, so that the different vertical sheets interlocked to form a stable downward-growing crystal matrix. During

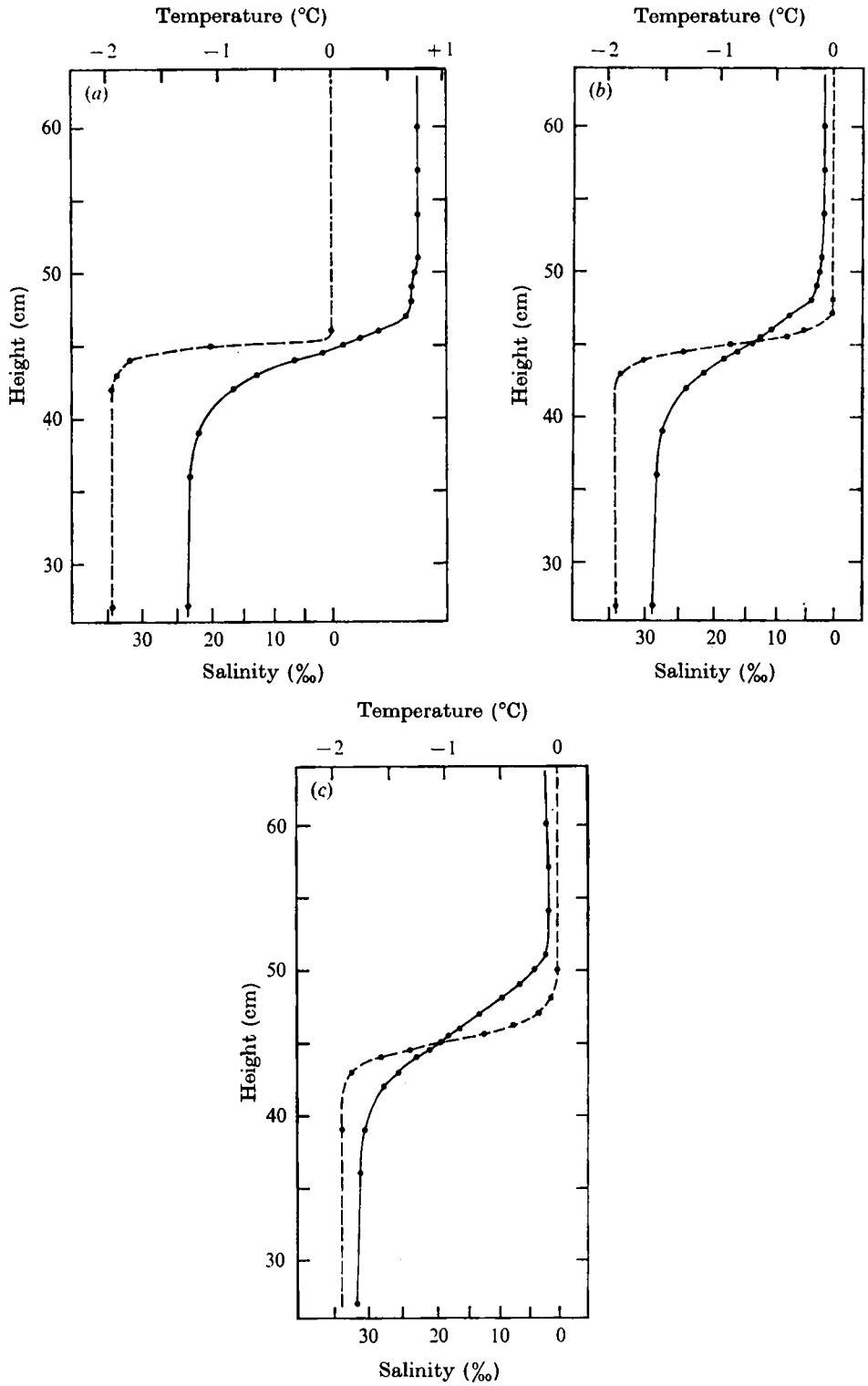

FIGURE 9. Observed temperature and salinity profiles. ●, measured points; ——, connects the temperature measurements; – – –, connects the salinity measurements. To show when supercooling occurs, we plot salinity as the freezing temperature of its solution. This causes the slight scale distortion at the bottom of the figure. (*a*) The initial conditions; day 1, 1500 h; (*b*) day 2, 1030 h; (*c*) day 3, 1500 h.

this phase of the experiment, the crystals grew down at a rate of $3–5 \times 10^{-1}$ cm h^{-1}. In summary, although we have no direct observations of the form that convection takes in the fresh-water layer, the indirect evidence of the presence of supercooled water at the interface, the downward growth of the crystal layer, and the supercritical value of $R_{a\delta}$ strongly suggests that convection occurs.

From our observations, we can also estimate the ratio of the heat transferred by the convective instability to the conductive heat transfer in the analogous thermal diffusion layer. To make this estimate, we first approximate the boundary conditions on the fresh-water layer in our tank as follows: at the plane $z = 0$ beginning at time $t = 0$, we hold the temperature and salinity constant at $T = T_0$ and $s = s_0$ respectively. Far from the interface, the salinity boundary condition is $s \to 0$ as $z \to \infty$, so that, from CJ, the solution of the salt diffusion equation is

$$s = s_0 \operatorname{erfc}[z/2(Dt)^{\frac{1}{2}}]. \tag{3}$$

As figures 9 (*b*) and (*c*) show, the observed salinity profile qualitatively resembles the error-function profile (3) whereas the temperature decreases nearly linearly across the transition layer. There are two reasons for the different behaviour of the temperature. First, the presence of the convective instability means that, for $s_0 \gtrsim 10^{-1}$‰, the water is unstably stratified, so that the heavier warmer water constantly replaces the lighter supercooled water. Therefore, at the top of the salinity transition layer, the temperature is approximately constant at 0 °C.

Second, the temperature field adjusts to a change in boundary conditions across the salinity layer in the diffusion time $z_s^2\kappa^{-1}$, where z_s is the salinity-layer thickness, or much faster than the speed at which the salinity layer diffuses. To show this, if we choose $s = 0{\cdot}05$‰ as a salinity characteristic of the upper edge of the salinity layer, then from (3),

$$z_s = 4{\cdot}4(Dt)^{\frac{1}{2}} \tag{4}$$

for the experimental value of $s_0 = 34$‰. From (4), in the time $z_s^2\kappa^{-1}$, z_s changes by the amount

$$\delta z_s/z_s = \tfrac{1}{2}(4{\cdot}4)^2/\alpha_1 = 0{\cdot}05, \tag{5}$$

or by only 5%. Therefore, given both (5) and the approximately constant temperatures of T_0 and 0 °C at the bottom and top of the salinity layer, we expect a steady temperature distribution in the transition layer, which for one-dimensional flow gives a linear profile.

For this case, the heat flux across the plane $z = 0$ is

$$F \cong -kT_0/z_s.$$

For the purely diffusive case of a temperature T_0 imposed at both $z = 0$ and time $t = 0$ which diffuses into 0 °C water without convection, the heat flux across $z = 0$ from CJ is

$$F' = -kT_0/(\pi\kappa t)^{\frac{1}{2}}. \tag{6}$$

Therefore the Nusselt number for this phase of our experiment is

$$N_u = \frac{F}{F'} = \frac{(\pi\kappa)^{\frac{1}{2}}}{4{\cdot}4\,D^{\frac{1}{2}}} \cong 5,$$

so that the convective instability increases the heat transfer from the fresh to the salt water by a factor of 5 over the classic heat diffusion case.

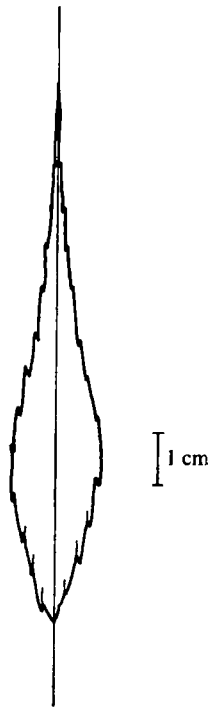

FIGURE 10. The observed cross-sectional profile of a typical crystal.

4. Lateral growth at the interface

In the experiment, the convective phase ended when the thin vertical sheets of ice shown in figure 5(*d*) suddenly formed on both the Plexiglas walls and the thermocouple mount at those depths where previously we had observed supercooled water. After this ice formation, the downward growth rate of the crystal matrix decreased to about 1 cm day^{-1}, and most of the new ice grew laterally from the existing crystals at the interface.

As the experiment progressed, the interfacial ice formed in two ways. First, new vertical sheets with a width of order 10^{-1} cm and the thickness shown in figure 6 occasionally grew laterally away from the original sheets to fill in the tank interior. For example, four days after the interfacial ice formation, we found that a rectangular cross made up of two sheets had subdivided the interior into four parts of roughly equal areas. As time went on, the growth of additional sheets further subdivided the interior. Because of the difficulty of observing horizontal growth inside the tank, we were unable to measure the rate of this growth; however, sheets with a length of 10–30 cm appeared in the tank over the period of a day.

Second, both the existing and new sheets, which immediately after their formation were of nearly uniform width, grew laterally with velocities of order 10^{-1} cm day^{-1} to produce a characteristic crystal shape. Figure 10, a qualitative sketch of a typical crystal cross-section observed five days after the interfacial

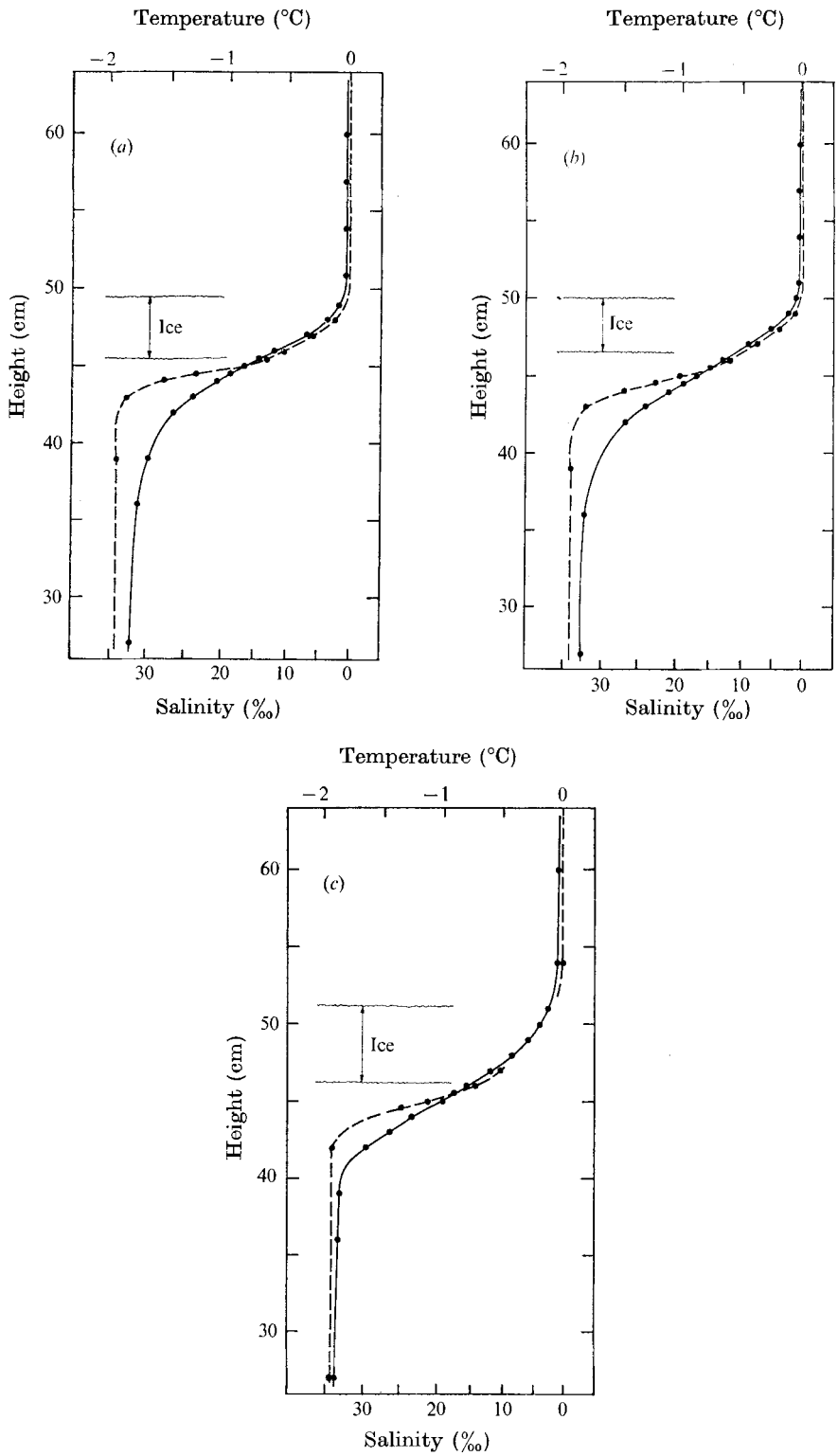

FIGURE 11. Observed temperature and salinity profiles. See legend to figure 9. (*a*) Day 4, 1500 h; (*b*) day 6, 1730 h; (*c*) day 10.

ice formation, shows the blunt pointed tip, broad middle and gradually tapered upper portion of the crystal which were characteristic of this lateral growth. Both the formation of new sheets and the lateral crystal growth continued until a rough-bottomed horizontal ice sheet separated the fresh from the salt water.

For this phase of the experiment, figure 11 displays three typical s and T profiles on which we also show the approximate vertical extent of region of lateral ice growth. To interpret these profiles, we note that, during the period covered by the profiles, the ice sheet which formed just behind the thermocouples on the mount grew laterally over the thermocouples at a rate of order 10^{-1} cm day^{-1}. Therefore, the temperatures shown in figure 11 were recorded very near the ice–water boundary. On the other hand, we drew the salinity samples away from the immediate vicinity of the ice, so that, because of selective withdrawal, the salinities shown in figure 11 are horizontal averages at each depth. The profiles in figure 11 show that above the level of ice formation s and T lie nearly on the same curve, so that the temperature near the ice–water interface nearly equals the average freezing point at that depth.

On the assumption that, above the depth of the ice in the tank, s and T diffuse at the same rate and are functions only of depth, we can derive a simple theory describing the shape and growth rate of the individual crystals. Before deriving this theory, we first discuss the physics of the lateral growth, then carry out a scale analysis.

At an ice–salt-water interface, the eutectic or freezing condition for our range of salinities is

$$T = -ms, \tag{7}$$

where $m = 5{\cdot}3 \times 10^{-2}$ °C for s measured in ‰ (from Kaufman 1960, table 50). Therefore, adjacent to a vertical ice wall, s and T must diffuse at the same rate. Far from an ice wall, or without one, the previous section shows that T diffuses an order of magnitude faster than s, so that supercooling occurs. For s and T to diffuse at the same rate near a vertical ice wall, the wall must grow laterally to heat the fluid and thereby remove the supercooling.

Furthermore, for growth velocities less than 10^{-4} cm s^{-1} or 10 cm day^{-1}, Weeks & Lofgren (1967) show that ice grown from salt solutions is very nearly fresh ice, with the excess salt rejected into the solution. Therefore, the growing ice wall serves as both a known salt and heat source. For example, from our thermocouple record, the initial interfacial ice growth took place in about 2 h beginning at 1900 h on day 3. A detailed comparison of the profiles of figures 9(*c*) and 11(*a*), which were taken respectively 4 h before and 20 h after this ice growth, shows that the growth both warmed the water and made it more salty.

To model the lateral crystal growth, we consider the problem of a fluid stratified in both s and T contained between parallel vertical ice walls with the eutectic condition (7) valid at the walls. If the fluid away from the walls adjusts so rapidly to the side-wall sources of heat and salt that s and T are horizontally uniform, then we may treat the ice walls as *volume* sources of heat and salt, and solve for the crystal shape from a simple one-dimensional model. To see when this model is valid, we next estimate the maximum horizontal plate separation for which s and T are horizontally uniform.

Veronis (1970) shows that a fluid which is stratified in a single component and contained between vertical walls adjusts to small changes in the component at the walls through 'buoyancy layers', which are the stratified-fluid equivalent of Ekman layers. For our experiment, the previous section showed that the density is very nearly independent of temperature, so that s controls the density. Therefore, following Veronis, the salinity time scale t_s for the interior to adjust to side-wall changes in salinity is

$$t_s \sim N^{-1}(\nu/D)^{\frac{1}{2}} R_a^{\frac{1}{4}}, \tag{8}$$

where N is the Väisälä frequency,

$$N^2 \simeq g\Delta\rho/d\rho,$$

and R_a is the Rayleigh number

$$R_a = N^2(2a)^4/\nu D.$$

In the above, $\Delta\rho$ is the density difference across the stratified layer, $2a$ is the horizontal separation of the side walls and d is the vertical thickness of the stratified layer.

The interior temperature field adjusts to changes in side-wall conditions in two ways. First, since temperature has only a negligible effect on density, there will not be a separate buoyancy layer for heat, rather the salinity layers will advect some heat away from the walls. Second, heat diffusion will transfer heat from the walls to the interior. For scaling purposes, we neglect heat advection and assume that diffusion controls the temperature time scale t_T on which the interior adjusts to a change in side-wall temperature. For two vertical parallel boundaries separated by a distance $2a$ in the horizontal, CJ (§ 3.3) shows that the temperature adjustment time scale is

$$t_T = a^2\kappa^{-1}.$$

To solve for the maximum plate separation for which the s and T are functions only of z, we compare the horizontal time scales t_s and t_T with the vertical diffusion time scales. For a stratified layer of thickness d, the time scales characteristic of the vertical salt and heat diffusion are d^2D^{-1} and $d^2\kappa^{-1}$ respectively.

The salinity field will be one-dimensional if $t_s \ll d^2D^{-1}$, or from (8) if

$$a \ll d^2N^{\frac{1}{2}}/2(\nu D)^{\frac{1}{4}}. \tag{9a}$$

For our experiment, $d \sim 10\,\text{cm}$ and $\Delta\rho \sim 10^{-2}\,\text{gm cm}^{-3}$, so that $N \sim 1\,\text{s}^{-1}$. Substitution of these values along with the values of ν and D given in the text into (9a) shows that s will be one-dimensional if $a \ll 10^3\,\text{cm}$; a condition which our experiment satisfies.

Similarly, T is one-dimensional if $t_T \ll d^2\kappa^{-1}$, or if

$$(a/d)^2 \ll 1. \tag{9b}$$

For $d = 10\,\text{cm}$, $(a/d)^2$ is of order 10^{-1} if $a = 2{\cdot}5\,\text{cm}$, so that the temperature condition (9b) is much more restrictive than (9a). If $a \gtrsim d$, we expect both supercooling away from the walls and some additional heat transfer from the walls; this statement is consistent with our observations of new crystals forming in the tank interior.

To analyse the ice growth under the restrictions (9), we assume that thin parallel vertical ice sheets, of negligible heat capacity and a characteristic spacing $2a$, extend from $z = 0$ to $z = \infty$. Further, on the assumption that the ratio of the volume of ice to the volume of fluid is negligible, we neglect the effects of the ice conductivity and its heat capacity. We also neglect any convection driven by the volume change of the ice upon freezing, and because the observed growth velocity is so small, we assume that the new ice is fresh-water ice. From Kaufman (1960) and CJ, the water has a thermal conductivity $k = 1{\cdot}4 \times 10^{-3}\,\mathrm{cal\,cm^{-1}\,s^{-1}\,°C^{-1}}$ and a specific heat $c_p = 1{\cdot}0\,\mathrm{cal\,gm^{-1}\,°C^{-1}}$; the ice has a latent heat $L = 80\,\mathrm{cal\,g^{-1}}$ and density $\rho_i = 0{\cdot}92\,\mathrm{g\,cm^{-3}}$. Since figure 6 shows that during this phase of the experiment the bottoms of the ice crystals remained very nearly at the same depth, we use as one of our boundary conditions that, at $z = 0$, s and T are constant at some point on the freezing curve. The other condition is that the eutectic condition (7) holds at the walls.

For one-dimensional diffusion CJ shows that the relevant diffusion equations with volume sources of heat and salt are

$$\mathscr{L}_\kappa T = A(z,t)/\rho c_p \tag{10a}$$

and

$$\mathscr{L}_D s = B(z,t), \tag{10b}$$

where

$$\mathscr{L}_{(\kappa,D)} = \partial/\partial t - (\kappa, D)\,\partial^2/\partial z^2$$

is the diffusion operator with κ and D assumed constant, and A and B are respectively the source terms for heat and salt.

From CJ (§ 1.6) the heat source term is

$$A = \frac{L\rho_i}{a}\frac{\partial \eta}{\partial t}, \tag{11a}$$

where $\eta(z,t)$ gives the crystal profile. Similarly, from Frank (1950) the salt source term for the growth of fresh ice is

$$B = \frac{s(z,t)}{a}\frac{\partial \eta}{\partial t}, \tag{11b}$$

so that the salinity $s(z,t)$ is the solute equivalent of the latent heat.

Substitution of (7) and (11) into (10) gives the following equation for s:

$$\mathscr{L}_D s = -s[\rho c_p m/L\rho_i]\,\mathscr{L}_\kappa s. \tag{12}$$

To simplify the subsequent analysis, we write the boundary conditions on (12) as

$$s = 2s_1 \quad \text{at} \quad z = 0, \tag{13a}$$

$$s \to 0 \quad \text{as} \quad z \to \infty, \tag{13b}$$

where s_1 is the mean salinity of the water above the ice–water interface. In our experiment, $s_1 = 8{\cdot}5‰$, which corresponds to a freezing-point depression $\Delta T_1 = 0{\cdot}45\,°\mathrm{C}$. Further, we write s in the non-dimensional form

$$s = s_1(1+\theta), \tag{14}$$

so that (13) becomes

$$\theta = 1 \quad \text{at} \quad z = 0, \tag{15a}$$

$$\theta \to -1 \quad \text{as} \quad z \to \infty. \tag{15b}$$

Two non-dimensional parameters characterize the crystal growth problem. First, the ratio α_1 of the diffusivities defined in (1); second, the parameter

$$\alpha_2 = \Delta T_1 \rho c_p / L \rho_i = \Delta T_1 k / \kappa L \rho_i, \tag{16}$$

which is the ratio of the volume of ice formed to the volume of water heated through ΔT_1 by the rejected latent heat. In our experiment, $\alpha_2 = 5{\cdot}3 \times 10^{-3}$. The product

$$\alpha_3 = \alpha_1 \alpha_2$$

also appears in the analysis; its experimental value is $\alpha_3 = 1{\cdot}0$.

Substitution of (1), (14) and (16) into (12) and neglect of terms of order α_2 gives

$$D(1+\alpha_3)\,\theta_{zz}\left(1+\frac{\alpha_3}{1+\alpha_3}\,\theta\right) = \dot{\theta}, \tag{17}$$

where the subscript z and superscript dot represent differentiation with respect to z and t. Therefore, we define both a new diffusivity

$$D' = D(1+\alpha_3), \tag{18a}$$

where $D' = 2D$ for the experiment, and a perturbation parameter

$$\epsilon = \alpha_3/(1+\alpha_3) = 0{\cdot}5, \tag{18b}$$

so that (17) becomes

$$D'\theta_{zz}(1+\epsilon\theta) = \dot{\theta}. \tag{19}$$

Equation (19) is a nonlinear form of the diffusion equation. Its form suggests that the solution may be represented as a regular perturbation series about $\epsilon = 0$. In the limit of small ϵ, the only effect of the vertical ice sheets is to increase the diffusivity D according to (18a). In the subsequent analysis, we shall calculate both the crystal shape and the vertical heat flux from the linearized form of (19).

If we again assume a steplike θ profile at $t = 0$, then the classic solution of the linearized equation (19) is

$$\theta = 1 - 2\,\mathrm{erf}\,u, \tag{20}$$

where $u = z/2(D't)^{\frac{1}{2}}$. From (7), (10$a$), (11$a$) and (14), the lateral crystal growth is

$$\dot{\eta} = -a\alpha_2 \mathscr{L}_\kappa \theta. \tag{21}$$

Substitution of (20) into (21) gives, to order α_1^{-1},

$$\dot{\eta} = -2a\alpha_2 \frac{\kappa}{D'} \frac{\partial}{\partial t}\{\mathrm{erf}\,u\}. \tag{22}$$

To calculate the crystal shape, we approximate the initial salinity profile above the ice–water interface in this phase of the experiment as equation (20) with the argument u_1 based on $t_1 = 3$ days. Therefore, from (22), the crystal shape at a later time is simply

$$\eta = 2a\alpha_2 \kappa D'^{-1}(\mathrm{erf}\,u_1 - \mathrm{erf}\,u_2). \tag{23}$$

In order to compare the crystal profile (23) with the observed profile in figure 10, we set $t_2 = 8$ days and $a = 5\,\mathrm{cm}$, where we choose the value of a so that the

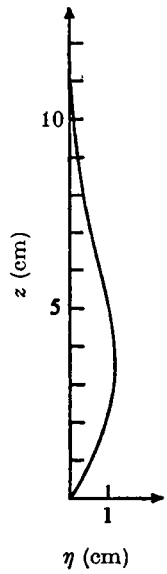

FIGURE 12. The calculated crystal profile for the conditions given in the text.

calculated and observed profiles have the same thickness, and plot the result in figure 12. The calculated profile obviously resembles the observed one.

We next calculate the heat flux F across the plane $z = 0$ generated by the lateral crystal growth, where

$$F = -k[\partial T/\partial z]_{z=0}. \tag{24}$$

Substitution of (7), (14) and (20) into (24) gives

$$F = -k2\Delta T_1/(\pi D't)^{\frac{1}{2}}, \tag{25}$$

where $2\Delta T_1$ is the total temperature difference across the crystal sheets. Comparison of (25) with the heat flux F' from the classic heat diffusion model in (6) gives

$$N_u = F/F' = (\kappa/D')^{\frac{1}{2}}, \tag{26}$$

and substitution of the experimental parameters into (26) gives $N_u \simeq 10$. Therefore, the presence of the vertical crystals increases the heat transfer by an order of magnitude over the classic case.

In the ocean, because the horizontal scales of the oceanic under-ice melt ponds in some cases are much greater than the width of our tank, the lateral growth phase may occur differently. Campbell's observations suggest that, inside at least one pond, the convective phase continued until the vertical crystal layer grew down to the interfacial supercooled water. Because the horizontal spacing of this crystal layer is of order 1 cm, the solid horizontal ice sheet may form more rapidly in some oceanic cases than in our experiment.

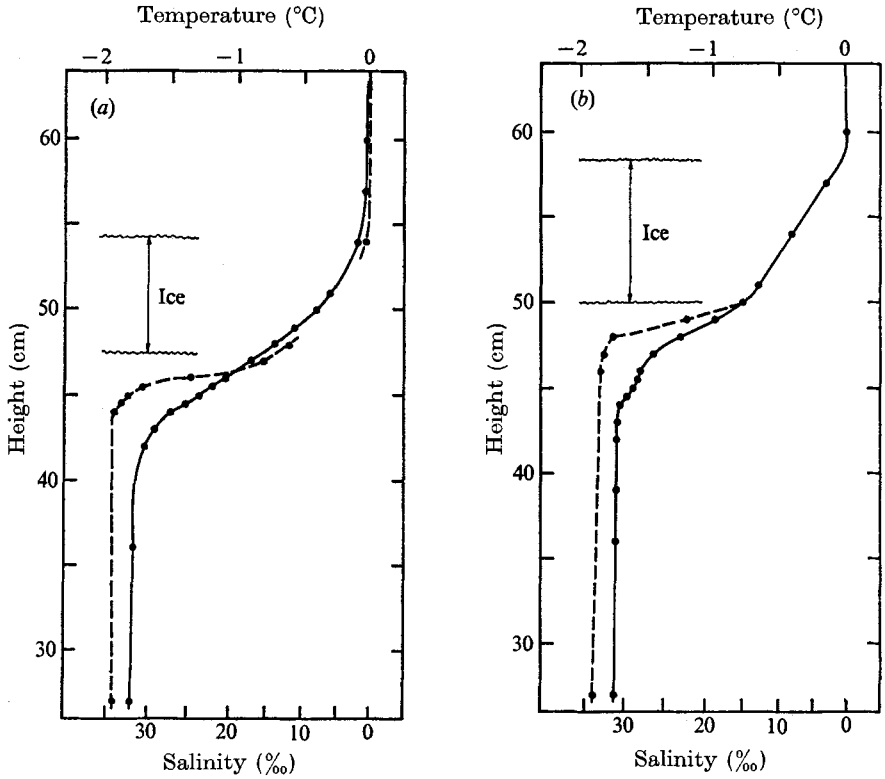

FIGURE 13. Observed temperature and salinity profiles. See legend to figure 9. (*a*) Day 17; (*b*) day 25.

5. Migration of the ice sheet

The third phase of the experiment begins with the formation of a solid horizontal ice sheet from the laterally growing crystals. As figure 6 shows, once this ice sheet forms, it migrates slowly upwards. To understand this migration, we examine the temperature and salinity profiles.

Figure 13 shows two characteristic temperature and salinity profiles from the period of the upward migration. Figure 13(*a*) shows a profile from the period when the ice sheet had an irregular bottom; figure 13(*b*), that when the ice had a flat bottom. In the following analysis, we restrict our attention to the flat-bottomed case. Inside the ice sheet, from figure 13(*b*), the temperature has a linear profile, with a slope change at the top and bottom. Ice formation at the top causes the upper slope change. The heat released by this freezing flows through the ice to the lower interface, where it tends to warm the lower interface slightly above the freezing curve (7). To restore equilibrium, the lower surface melts, thus cooling and diluting the adjacent water back to the freezing curve. This melting absorbs heat, thus causing both the lower slope change in figure 13(*b*) and the ice sheet migration.

For the flat-bottomed ice, we shall calculate both its net accretion and its migration rate as a function of the salt and heat fluxes in the salt water. We

again use a one-dimensional co-ordinate system, where z_1 is the height of the lower interface above some arbitrary origin and z_2 is the height of the upper interface. At the upper interface, the fresh-water temperature is 0 °C; at the lower, the temperature and salinity are T_w and s_w respectively. The ice has a thermal conductivity $k_i = 5{\cdot}3 \times 10^{-3}\,\mathrm{cal\,cm^{-1}\,s^{-1}\,°C^{-1}}$ and a specific heat $c_{pi} = 0{\cdot}50\,\mathrm{cal\,g^{-1}\,°C^{-1}}$. Because crystals loosely fill the fresh water above the ice sheet, for a given volume of this ice–water mixture, the apparent latent heat is less at the upper interface than at the lower. Therefore, at the upper interface we define the latent heat L_2 as

$$L_2 = L(1-\gamma),$$

where γ is a constant of order 10^{-1}.

The following boundary conditions describe the ice sheet migration. At the upper interface, freezing generates all the heat flow through the ice, so that the boundary condition is

$$k_i T_{iz} = +\rho_i L_2 \dot{z}_2 \quad \text{at} \quad z = z_2, \tag{27}$$

where the subscript i refers to the ice.

At the lower interface, we have three boundary conditions. First, the salt water must satisfy the eutectic condition (7) at $z = z_1$. Second, the thermal boundary condition is

$$k_i T_{iz} = +\rho_i L \dot{z}_1 + k T_z \quad \text{at} \quad z = z_1, \tag{28}$$

where the first term is the heat flux through the ice; the second, the heat absorbed by melting; the third, the heat transmitted to the salt water.

Third, on the assumption of steady motion of the lower interface, from Frank (1950), the salinity boundary condition is

$$\dot{z}_1 = -(D/s_w)\, s_z \quad \text{at} \quad z = z_1. \tag{29}$$

In the ice interior, we assume that the ice thickness changes so slowly that the temperature profile is linear. As both figure 13(*b*) and other undisplayed profiles show, our observations support this assumption. Therefore,

$$T_{iz} = -T_w/(z_2 - z_i) \quad \text{for} \quad z_1 \leqslant z \leqslant z_2. \tag{30}$$

Substitution of (27) and (30) into (28) gives the following equation for the net ice accretion Δz:

$$[(1-\gamma)\,\dot{z}_2 - \dot{z}_1] = \Delta \dot{z} = (k/L\rho_i)\, T_z. \tag{31}$$

Equations (29) and (31) plus the eutectic condition (7) give both the net accretion of the ice sheet and its upward motion in terms of the temperature and salinity gradients in the salt water. The initial condition on these equations would be that, at some time $t = 0$, the ice sheet has a finite thickness determined by the end result of the lateral crystal growth described in § 4. Obviously, to solve for the ice growth, we must make various assumptions about T_z and s_z in the salt water. Because there are no measurements of these gradients under summer pack ice, and since the experiment does not suggest a simple solution, we leave the equations in the above form.

6. Concluding remarks

In summary, the mathematical models of the processes which lead up to the formation of a solid ice sheet between a fresh-water and a salt-water layer at their respective freezing points show that the heat transfer is 5-10 times more efficient than for classic heat diffusion. In the polar oceans, this model provides an efficient way for growing new ice in the summer from the temperature difference between the fresh-water surface run-off and the colder ocean water.

We thank Arnold Hanson for suggesting this problem and Paul LeBlond for pointing out the occurrence of this phenomena under the Ward Hunt Ice Shelf. We gratefully acknowledge the support of the Office of Naval Research under Project NR307-252 and Contract N00014-67-A-0103-0007, Contribution 754 of the Department of Oceanography, University of Washington and Contribution 303 of the Department of Atmospheric Sciences, University of Washington.

REFERENCES

CARSLAW, H. S. & JAEGER, J. C. 1959 Conduction of Heat in Solids, 2nd edn. Oxford University Press.

FRANK, F. C. 1950 Radially symmetric phase growth controlled by diffusion. *Proc. Roy. Soc.* A 201, 586–599.

HANSON, A. N. 1965 Studies of the mass budget of Arctic pack-ice floes. *J. Glaciol.* 5, 701-709.

HODGMAN, C. D. (ed.) *1955 Handbook of Chemistry and Physics,* 37th edn. Cleveland: Chemical Rubber Publishing Co.

HOWARD, L. N. 1966 Convection at high Rayleigh number. *Proc.* 11th *Int. Congr. Appl. Mech., Munich* (ed. H. Görtler), pp. 1109-1115. Springer.

KAUFMAN, D. W. (ed.) 1960 *Sodium Chloride.* Reinhold.

LYONS, J. B., SAVIN, S. M. & TAMBURI, A. J. 1971 Basement ice, Ward Hunt Ice Shelf, Ellesmere Island, Canada. *J. Glaciol.* 10, 93-100.

MOWBRAY, D. E. 1967 The use of schlieren and shadowgraph techniques in the study of flow patterns in density stratified fluids. *J. Fluid Mech.* 27, 595–608.

NANSEN, F. 1897 *Farthest* North, vol. 1, pp. 457-459. New York: Harper & Brothers.

PERRY, R. H., CHILTON, C. H. & KIRKPATRICK, S. D. (eds.) 1963 *Chemical Engineers' Handbook.* McGraw-Hill.

TURNER, J. S. 1973 *Buoyancy Effects* in Fluids. Cambridge University Press.

UNTERSTEINER, N. 1967 Natural desalination and equilibrium salinity profile of old sea ice. In *Physics of Snow and Ice* (ed. H. Oura), vol. 1, pp. 569-577. Institute of Low Temperature Science, Hokkaido University, Japan.

UNTERSTEINER, N. & BADGLEY, F. I. 1958 Preliminary results of thermal budget studies on Arctic pack ice during summer and autumn. In *Arctic Sea Ice,* pp. 85-92. Washington: U.S. Nat. Acad. Sci., Nat. Res. Counc. Publ. no. 598.

VERONIS, G. 1970 The analogy between rotating and stratified flows. Ann. *Rev. Fluid Mech.* 2, 37-66.

WEEKS, W. F. & LOFGREN, G. 1967 The effective solute distribution coefficient during the freezing of NaCl solutions. In *Physics of Snow and Ice* (ed. H. Oura), vol. 1, pp. 5'79-599. The Institute of Low Temperature Science, Hokkaido University, Japan.

ZUBOV, N. 1945 Arctic Ice (English trans.). U.S. Navy Electronics Laboratory, San Diego.

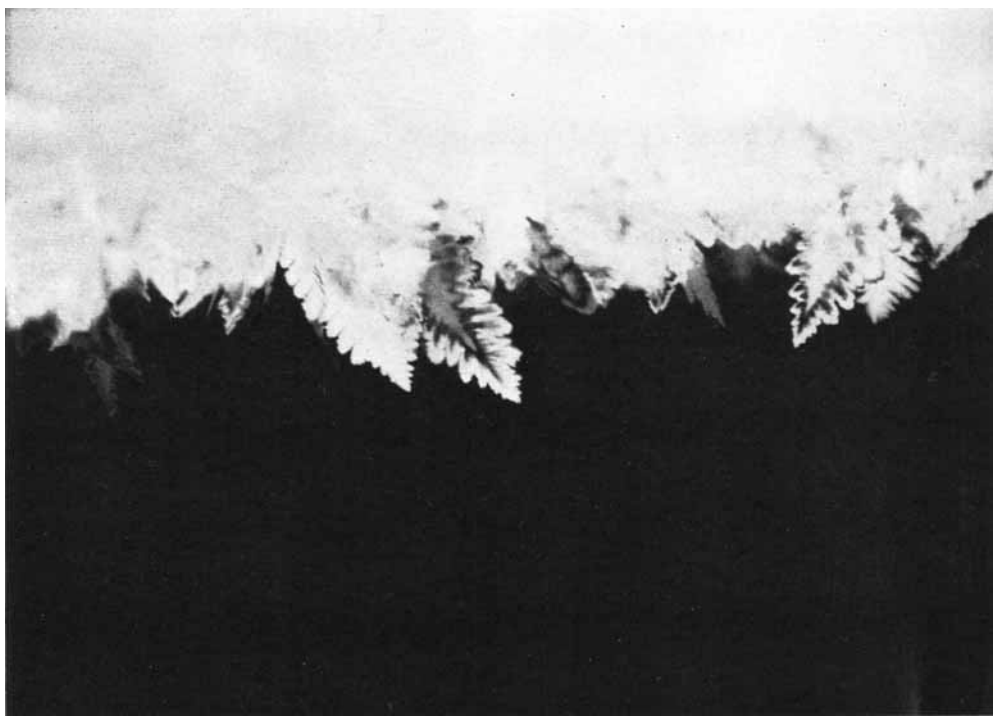

FIGURE 4. A close-up photograph of the ice crystals which initially formed in the experiment. The width of the large crystals is about 2 cm.

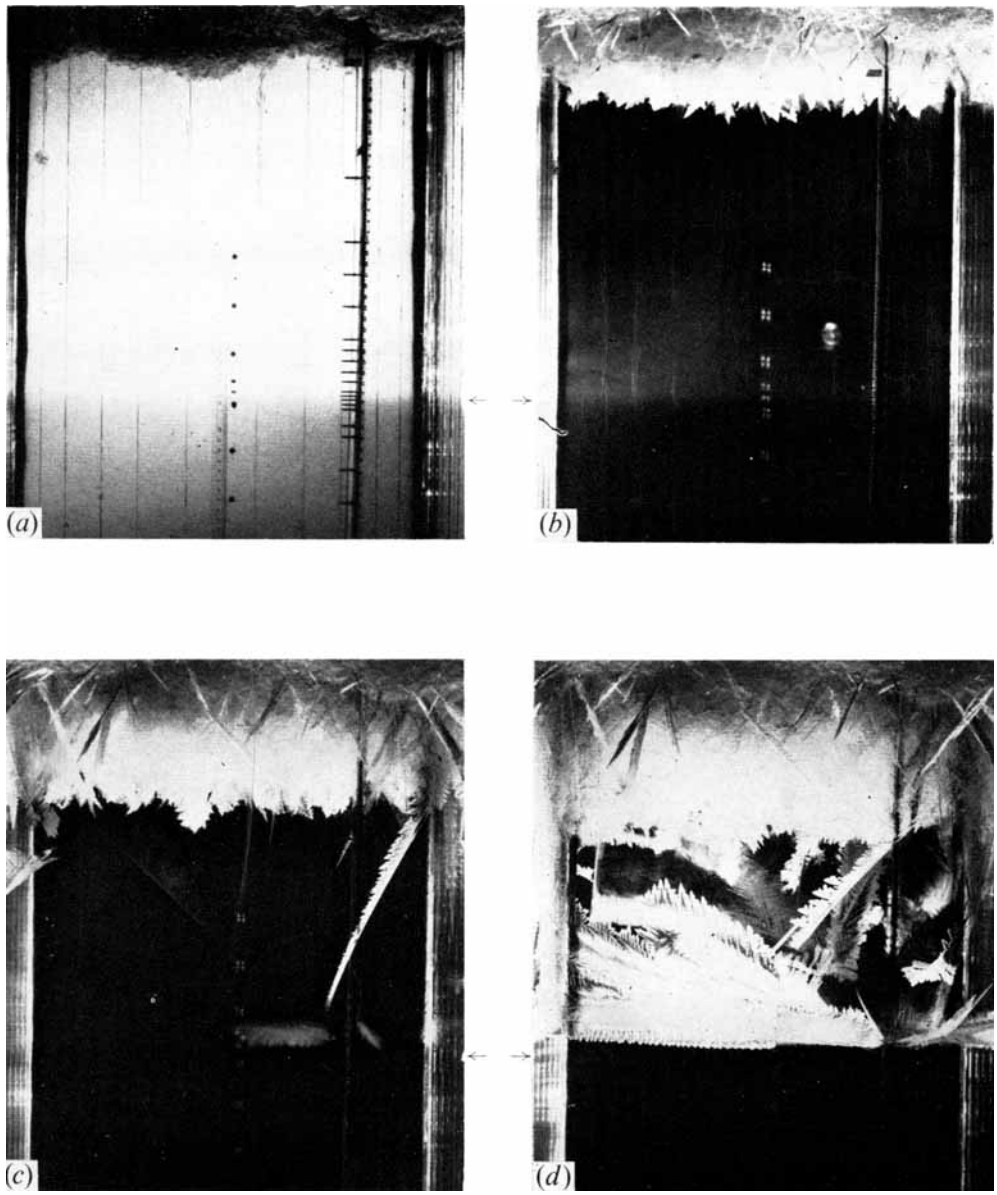

FIGURES 5(*a*–*d*). For legend see plate 3.

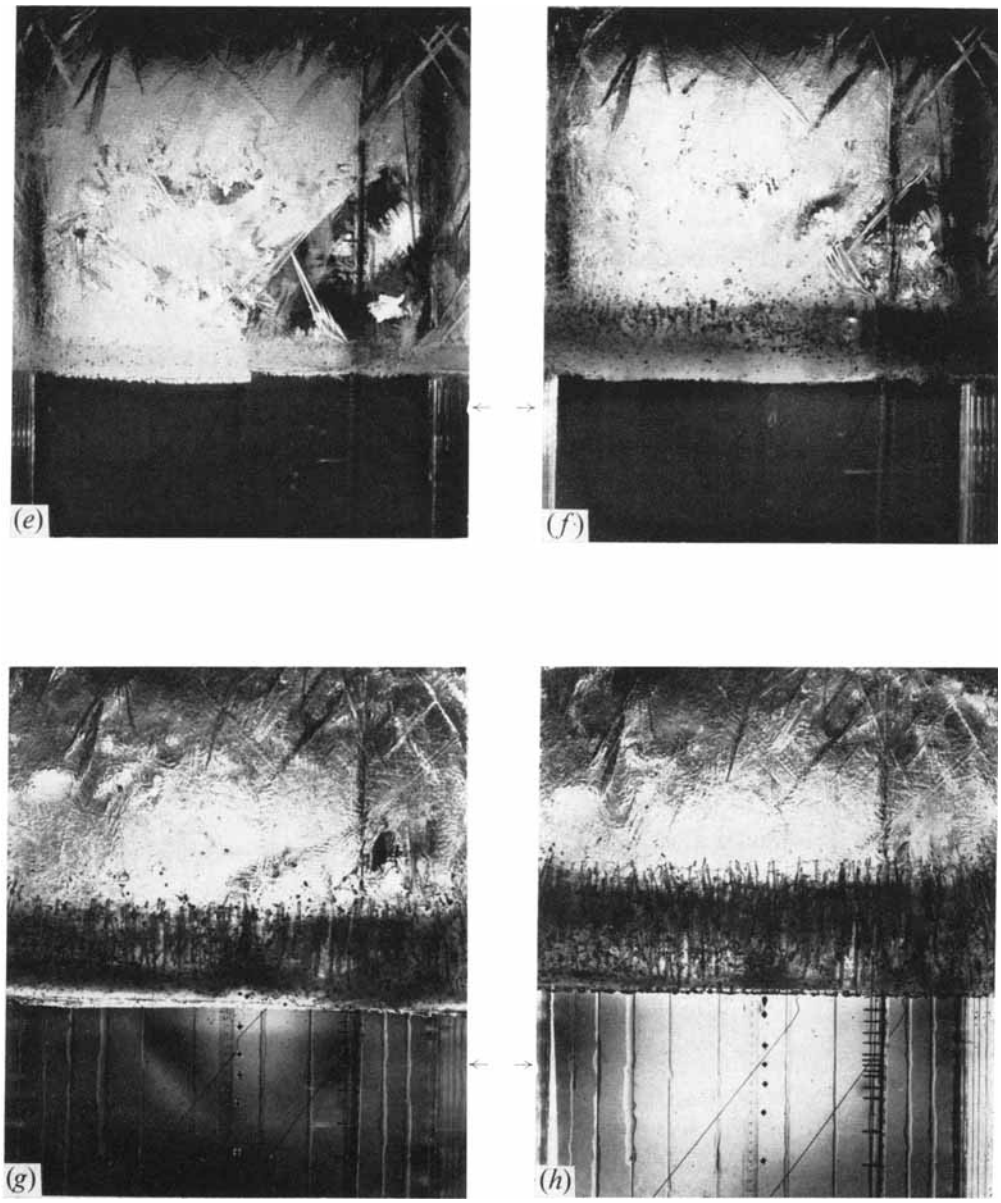

FIGURE 5. A sequence photographs of the ice growth. The regularly spaced vertical lines are on the back wall of the tank; the small horizontal arrows mark the initial position of the interface. (*a*) The initial conditions; day 1, 1500 h; (*b*) day 2, 1830 h; (*c*) day 3, 1400 h; (*d*) day 4, 1400 h; (*e*) day 6, 1800 h; (*f*) day 13; (*g*) day 22; (*h*) day 28.